Spectrochimica Acta Part A: Molecular and Biomolecular Spectroscopy xxx (xxxx) 121948

Contents lists available at ScienceDirect

Spectrochimica Acta Part A: Molecular and Biomolecular Spectroscopy

journal homepage: www.elsevier.com/locate/saa

A phase variety of fluorinated ionic liquids: Molecular conformational and crystal polymorph

Hiroshi Abe [a], Hiroaki Kishimura [a], Mikio Uruichi [b]

[a] Department of Materials Science and Engineering, National Defense Academy, Yokosuka 239-8686, Japan
[b] Institute for Molecular Science, Myodaiji, Okazaki 444-8585, Japan

ARTICLE INFO

Article history:
Received 21 August 2022
Received in revised form 26 September 2022
Accepted 3 October 2022

Keywords:
Fluorinated ionic liquid
Conformational polymorph
Crystal polymorph
Molecular flexibility

ABSTRACT

Crystal polymorphs of fluorinated ionic liquids (fILs) were examined at low-temperature (LT) by Raman spectroscopy. The fILs were 1-alkyl-3-methylimidazolium perfluorobutanesulfonate, [$C_n$mim][PFBS] (n = 4, 6, and 8). The cations and anions possess conformational degrees of freedom. Various LT phases were derived from the conformational polymorphs of the cations and the anions. Conformational flexibility depended on alkyl chain length. The crystal polymorphs in the fILs were sensitive to molecular conformations and flexibility.

1. Introduction

Molecular conformations in molecular systems have provided various crystal phases [1–6]. Degrees of freedom of molecular conformers are derived from intrinsic molecular structures and molecular flexibility (MF). MF is represented by a low-energy barrier on the potential energy surface [7]. Conformational polymorphs are directly connected with crystal polymorphs. Recently, to interpret crystal polymorphs, a crystal energy landscape (CEL) was introduced as a new concept [7–11]. Similar to the free energy landscape for supercooled liquid and amorphous [12], the CEL is expressed by comparable crystal energies in crystal polymorphs. Further, the crystal structure prediction using CEL is indispensable for screening pharmaceutical polymorphs [13–16]. Crystal polymorphs cause different physicochemical properties. Thus, crystal polymorph screening is an urgent issue to prevent changing drug properties.

Ionic liquids (ILs) have been used in designing structures and properties [17,18]. Novel functions such as nearly-zero vapor pressure for industrial applications were optimized from various combinations of cations and anions. Molecular conformations were determined by Raman spectroscopy (RS) combined with density functional theory (DFT) calculations [19]. In vibrational spectroscopy and DFT, liquid and crystal stabilities were clarified at low temperature (LT) and high pressure (HP). Particularly in the ILs, ionic interactions and packing efficiency associating with the molecular conformers were distinguished using the above powerful tool. Moreover, anion conformations having fluorination of the end groups have been examined from the design concept [21]. MF was estimated by nuclear magnetic resonance, X-ray diffraction (XRD) and computer-aided three-dimensional potential energy surface. The representative cation is 1-alkyl-3-methylimidazolium, $[C_n\text{mim}]^+$, where n reveals the alkyl chain length. Stable conformers of $[C_n\text{mim}]^+$ were calculated using DFT calculations [22–24]. By XRD, the crystal polymorphs of ILs were examined at LT and HP [25–37]. The LT crystal polymorphs differed from the HP ones. Moreover, multiple pathways of phase transitions (PTs) were observed in specific ILs at LT and HP.

The liquid structures of fluorinated ILs (fILs) were calculated using MD simulations [38]. The fILs were 1-alkyl-3-methylimidazolium perfluorobutanesulfonate ($[C_4F_9SO_3]^-$), [$C_n$mim][PFBS] ($2 \le n \le 12$). The hydrogenated and fluorinated chains of the fILs caused nanoheterogeneity, and polar and nonpolar nanodomains were visualized by the MD simulations. Resembling $[C_4F_9BF_3]^-$ [39], $[PFBS]^-$ possesses two stable conformations *trans* and *gauche* based on DFT calculations [33]. The PTs [$C_n$mim][PFBS] were examined at LT [33,40,41] and HP [36,37]. The PTs were characterized by crystal polymorphs. The fILs crystallizations imply that the molecular interaction between $[C_n\text{mim}]^+$ and $[PFBS]^-$ is predominant.

In this study, we investigated the relationship between the molecular conformational and crystal polymorphs of [$C_n$mim][PFBS] (n = 4, 6, and 8) at LT. Various molecular conformations of both cations and anion were clarified by RS.

https://doi.org/10.1016/j.saa.2022.121948
1386-1425/© 20XX

2. Experiments and simulations

The fILs used in this study were [C_4mim][PFBS] (FUJIFILM Wako Pure Chemical Co.) and [$C_n$mim][PFBS] (n = 6 and 8) (Kanto Chem. Co.). The molecular structures of [$C_n$mim]$^+$ cations and [PFBS]$^-$ anion were optimized by DFT (Fig. 1). Water in the fILs was removed by vacuum drying for a few days.

Raman spectra were measured using Via Reflex (RENISHAW). A 785-nm diode laser was used as an excitation source with a 0.35-mW power. Helium flow cryostat (Microstat He, Oxford) was installed to cool samples. The resolution of Raman spectroscopy was 1 cm^{-1}.

DFT calculations were performed to investigate the conformations and Raman bands of [$C_n$mim]$^+$ (n = 4, 6, and 8). All DFT calculations were performed using the B3LYP hybrid functional and 6–31 + + G(d,p) basis set of the *Firefly* package [42,43].

3. Results and discussion

The LT crystal polymorphs of [C_4mim][PFBS] were examined using simultaneous XRD and differential scanning calorimetry (DSC) measurements [33]. A series of PTs such as liquid → α → β → γ → β → liquid phases was clarified. Upon cooling, T_{C1} (=267 K), T_{C2} (=266 K), and T_{C3} (=249 K) were determined by the DSC thermal trace and XRD patterns. Upon heating, the inverse PT temperature (T_{C3} = 265 K) and melting point (T_m = 297 K) were probed. Obviously, hysteresis of the PTs appeared in the thermal cycle of [C_4mim][PFBS] [33] (Fig. S1). [C_4mim]$^+$ has four stable conformers [23] ntt, ngt, ng't, and ng'g' (Fig. 1) where n, t, g and g' denote *nonplanar*, *trans*, *gauche* and *gauche*', respectively. A ring deformation mode of [C_4mim]$^+$ appeared at around 600 cm^{-1} [44]. In the detailed DFT calculations [23], ntt, ng'g', ng't, and ngt were identified at 624.7, 597.7, 595.7, and 591.0 cm^{-1}, respectively. The energetical order was ng't < ng'g' < ngt < ntt [23]. Moreover, two conformers of [PFBS]$^-$ were optimized by DFT [33]. In [PFBS]$^-$, the Raman bands of the –SO_3 wagging mode were used to assign *trans* and *gauche* at 380.9 and 369.5 cm^{-1}, respectively (Fig. 1) [33]. Fig. 2 indicates the temperature dependences of Raman bands in [C_4mim][PFBS] upon cooling and heating using 785 nm. Upon cooling at 290 and 275 K, [C_4mim][PFBS] was in the liquid state, which was characterized by broad *trans* and *gauche* Raman bands of [C_4mim]$^+$. The *trans* and *gauche* conformers coexisted in the liquid state. [PFBS]$^-$ Raman bands in the liquid state were relatively sharp (Fig. 2). From the intensity ratio of the [PFBS]$^-$ Raman bands, the *trans* conformer was more favorable than the *gauche* conformer. By optical microscopy, crystallization occurred at 260 K. In the previous study [33], the DSC thermal trace indicates that T_{C1} (=267.1 K) and T_{C2} (=265.6 K) were close (Fig. S1). Thus, in the X-ray diffraction patterns, an α phase ($T_{C2} \le T \le T_{C1}$) was not detected due to the rapid α-β PT. In this study, the crystal at 260 K was in a β phase. At 260 K, sharp ntt, ngt, and ng't Raman bands were clearly decomposed by asymmetric profile fitting using the pseudo-Voigt function. Moreover, the *gauche* conformer of [PFBS]$^-$ increased in the β phase. By further cooling, a γ phase appeared at 230 K (Fig. 2). Below T_{C3}, the ntt conformer decreased drastically, whereas the ng'g' conformer became predominant. The ng'g' of [C_4mim]$^+$ is the typical folding conformer (Fig. 1). The smallest ntt Raman band (all *trans*) means that non-all *trans* (NAT) conformers were energetically selected at 230 K (T_{NAT}). Moreover, the *gauche* conformer of [PFBS]$^-$ almost vanished in the γ phase. Hence, the packing efficiency entirely differed in the *gauche* cation and *trans* anion of the γ phase. Compared with the HP crystal polymorph of [C_4mim][PFBS] [36], packing efficiency-preferred *gauche* [PFBS]$^-$ was detected slightly below 230 K. At ambient pressure, the NAT alkyl chain of [C_4mim]$^+$ could be well matched with *trans* [PFBS]$^-$. At 175 K, the Raman intensity ratio of [C_4mim][PFBS] changed extensively. Particularly, the ntt and the ng'g' Raman bands increased further, whereas the ngt band decreased. Because the minimum temperature (T_{min}) in a previous study [33] was 178 K, the above phase behavior was unobserved. Without XRD patterns, it is unclear whether the conformational change at 175 K corresponds to a PT. In addition, another conformational change was induced at 150 K. A small portion of the *gauche* [PFBS]$^-$ conformer remained, even at 100 K. The ntt Raman band of [C_4mim]$^+$ became the smallest at 100 K (Fig. 2). For [C_4mim][PF_6] [45], the NAT conformers also appeared in the crystals at lower temperatures. Thus, the NAT conformers of [C_4mim]$^+$ could be preferred at LT for higher packing efficiency. Moreover, the MF of cations and anion was clarified at LT. The NAT conformers of [C_4mim]$^+$ and *trans* dominant [PFBS]$^-$ at 100 K suggest that [C_4mim]$^+$ is more flexible than [PFBS]$^-$. At least, upon cooling, the complicated conformational polymorphs of both cations and anion in [C_4mim][PFBS] were obtained directly by RS. Meanwhile, upon heating, a distinct conformational change on the Raman spectra was detected at 260 K (Fig. 2). Apparent peak broadening occurred,

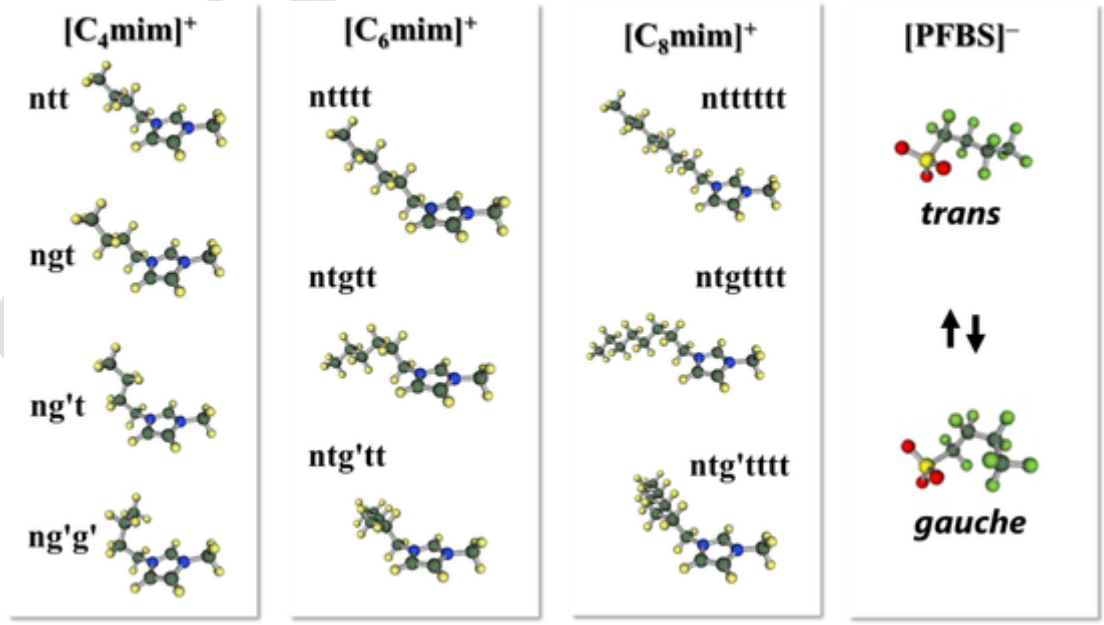

Fig. 1. Molecular conformations of [$C_n$mim]$^+$ (n = 4, 6, and 8) and [PFBS]$^-$, where n, t, g, and g' indicate *nonplanar*, *trans*, *gauche*, and *gauche*', respectively.

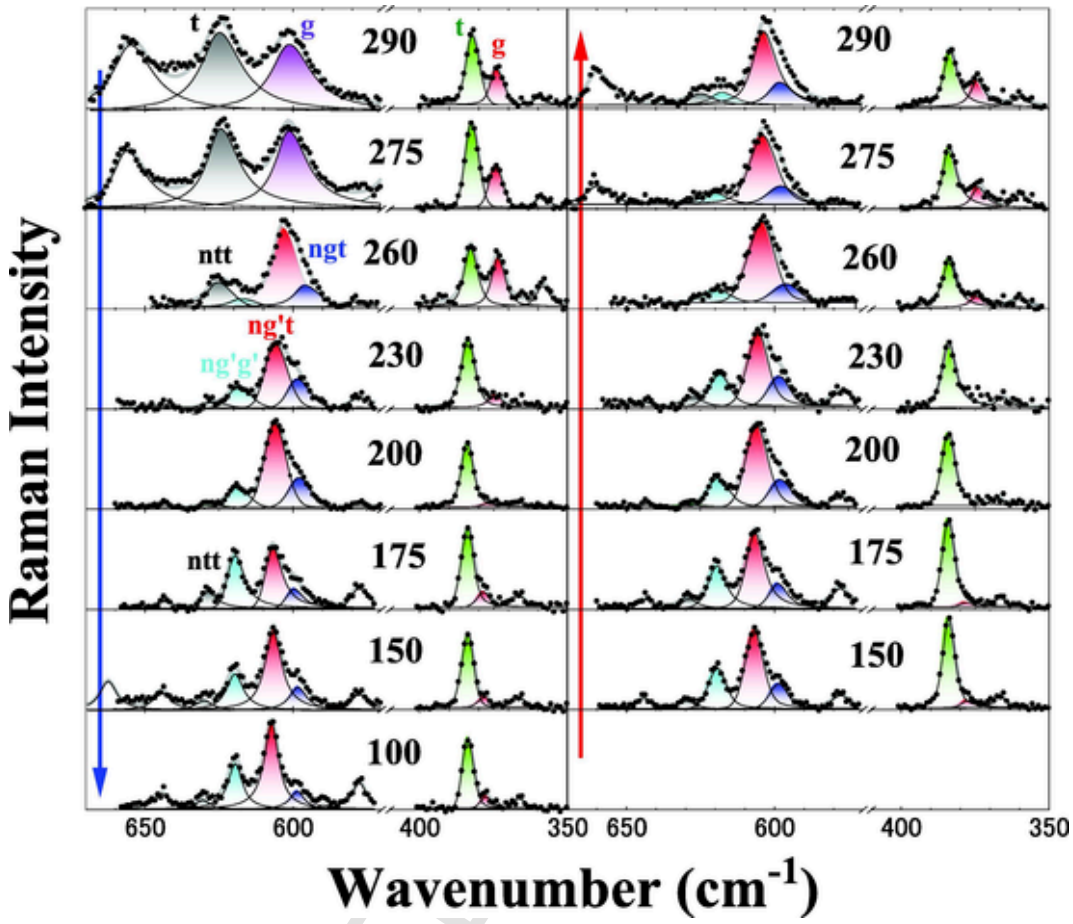

Fig. 2. Temperature dependences of Raman spectra of [C_4mim][PFBS] upon cooling and heating. Spectrum changes correspond to low temperature (LT) crystal polymorphs. The numbers in the figure indicate temperatures.

and the *gauche* conformer of $[PFBS]^-$ increased above 260 K. These modulations of the Raman profiles correspond to the reverse PT from the γ to β phase. Because T_m was 297 K, melting was unobserved in this study.

[C_6mim][PFBS] also indicated complicated LT crystal polymorphs [33]. In the DFT calculations, stable conformers of $[C_6mim]^+$ were found to be 15 [23]. In the previous study [22], energy difference (ΔE) was defined when ntttt is set to be 0 kJ/mol. For instance, conformers of $\Delta E < 0$ are ngttt, nggtt, nggtg, ng'ttt, ng'ttg, ng'ttg', ng'tgt, ng'tg't, ng'tg'g', ng'g'tt, ng'g'tg', and ng'g'g't (12 conformers). However, the calculated wavenumbers of some conformers are different from the observed ones. Even in $0 \leq \Delta E$, the wavenumbers of ntttt, ntgtt, and ntg'tt coincided with the observed ones. Among them, $[C_6mim]^+$ is classified into two: *trans*-like (ntg'tt, ntttt, and ntgtt) at around 625 cm^{-1}, and *gauche*-like (ng'g'tt, ng'g'tg', and ng'ttt) at around 600 cm^{-1}. The latter is much more stabilized than the former [23]. In the liquid state at 290 K, broad *trans* and *gauche* bands of $[C_6mim]^+$ were located at 625 and 600 cm^{-1}, respectively (Fig. 3). In addition, weak and broad Raman band existed in between them. The intermediated band, i, was not seen in $[C_4mim]^+$, and could be originated from the *trans* and *gauche* mixing conformers, such as ng'g'tt. One possible reason is that some additional fluctuations are superimposed by the crossover alkyl chain length ($n_c = 6$) from ionic to organic nature. In fact, the crossover behavior was enhanced in ILs-based mixtures [46,47]. Meanwhile, in the liquid state, the $[PFBS]^-$ conformer ratio in [C_6mim][PFBS] was comparable to that in [C_4mim][PFBS]. At 275 K, [C_6mim][PFBS] crystallized and crystal domains were observed by optical microscopy. One broad *trans* band was decomposed into three sharp bands: ntg'tt, ntttt, and ntgtt (Fig. 3). On the contrary, ng'g'tt, ng'g'tt, and ng'ttt bands at around 600 cm^{-1} were quite weak. In an α phase, the *trans*-based $[C_6mim]^+$ conformers occupied a unit cell. Upon cooling to 100 K, this tendency did not change on the Raman spectra. At 200 K, there was a drastic change in Raman bands at around 625 cm^{-1}. The ntg'tt conformer increased, and the peak became sharper. The *gauche* $[PFBS]^-$ conformer in [C_6mim][PFBS] completely vanished at 200 K, although the weak *gauche* band was obtained in [C_4mim][PFBS], even at 100 K. Thus, the *trans* $[PFBS]^-$ conformer was preferred in [C_6mim][PFBS] below 200 K. In the simultaneous XRD and DSC [33], T_{min} was 178 K due to the cooling limit (Fig. S1). From 200 K to 178 K, a distinct PT was not observed in the XRD patterns [33]. Hence, at 200 K, both cation and anion conformational changes occurred without a PT. By further cooling, the cation conformations drastically varied at 175 K, whose temperature was lower than T_{min} in XRD [33]. Thus, it is not confirmed that the conformational change is connected with a PT. Similar to [C_4mim][PFBS], below 175 K, the characteristic feature of the $[C_6mim]^+$ cation is represented by the smallest Raman band of ntttt (all *trans*). The NAT $[C_6mim]^+$ conformers occupied a unit cell below 175 K (T_{NAT}). Because the T_{NAT} of $[C_6mim]^+$ was lower than that of $[C_4mim]^+$, the alkyl chain bending or folding occurred more easily in [C_4mim][PFBS]. Upon cooling to 100 K, no conformational changes in [C_6mim][PFBS] were observed. Upon heating, the Raman bands at around 625 cm^{-1} obviously changed at 230 K (Fig. 3). Particularly, the ntttt band became the largest. Nevertheless, a PT at 230 K was undetected by XRD [33]. Further heating caused PT at T_{C3} (= 260 K). The γ phase was induced upon heating, although the γ phase was not formed upon cooling [33]. Moreover, above T_{C3}, the *gauche* $[PFBS]^-$ band was recovered. At T_{C4} (= 275 K), a δ phase, which differed from the α phase upon cooling [33], appeared. The ntgtt band was weakened at T_{C4}. Compared with

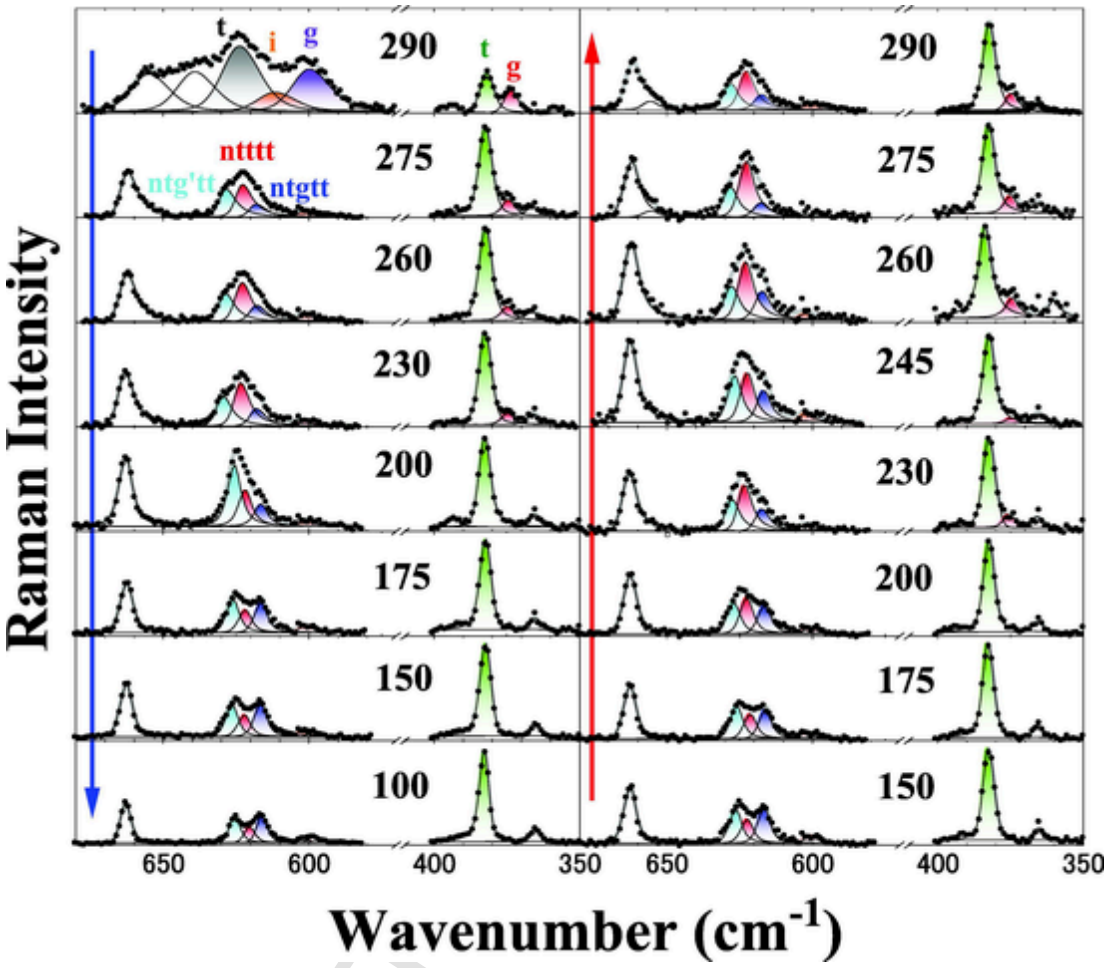

Fig. 3. Temperature dependences of Raman spectra of [C_6mim][PFBS] upon cooling and heating. Spectrum changes correspond to LT crystal polymorphs. The numbers in the figure indicate temperatures.

the Raman profile at 275 K upon cooling (α phase), the δ phase upon heating was expressed by a different Raman profile.

[C_8mim][PFBS] was a supercooled state at 290 K [33]. The *gauche* Raman band of [C_8mim]$^+$ at around 600 cm^{-1} was unobserved in the supercooled liquid (Fig. 4), implying that nonpolar nanodomains in supercooled [C_8mim][PFBS] comprise only the *trans*-like [C_8mim]$^+$ conformer. In the DFT calculations [24], stable ntttttt at 625.9 cm^{-1}, ng'ttttt at 597.0 cm^{-1}, and ngttttt at 592.3 cm^{-1} were evaluated. However, the ng'ttttt and ngttttt Raman bands did not exist in the supercooled liquid state. Therefore, the *gauche*-dominant conformers of [C_8mim]$^+$ were excluded at 290 K. In addition, *trans–gauche* conformer ratio of [PFBS]$^-$ differed from those of [C_4mim][PFBS] and [C_6mim][PFBS] in the supercooled liquid state. Therefore, no *gauche*-like [C_8mim]$^+$ bands and a small portion of the *gauche* [PFBS]$^-$ bands revealed the specific features in the supercooled liquid state of [C_8mim][PFBS]. The sudden profile change at 275 K ($< T_{C1}$) indicates the crystallization upon cooling, accompanied by the morphological change via optical microscopy. The α phase was characterized by a 2.4-nm-long lattice constant [33]. The broad 625-cm^{-1} band was split into three components at 275 K. By the DFT calculations, the ntg'tttt band at 627.0 cm^{-1}, nttttttband (all *trans*) at 625.9 cm^{-1}, and ntgtttt band at 625.3 cm^{-1} were assigned (Fig. 1). Both ntg'tttt and ntgtttt bands are regarded as the bending conformers (Fig. 1). Because the Raman bands at around 600 cm^{-1} were quite weak, the *gauche*-dominant conformers of [C_8mim]$^+$ existed slightly in a unit cell. At 215 K ($< T_{C2}$), the peak splitting of ntg'tttt and nttttttwas enlarged, and the *gauche* [PFBS]$^-$ band completely disappeared owing to an α-β PT [33]. Moreover, at 215 K, the all *trans* nttttttband was sufficiently large. In the β phase of [C_8mim][PFBS], the *trans* conformers in both [C_8mim]$^+$ and [PFBS]$^-$ occupied mainly unit cells. The β phase structure possessed an extremely long lattice constant of 5.2 nm, and the β crystal structure of [C_8mim][PFBS] was distinguished from others. To emphasize the peak splitting, the temperature dependences of the peak positions are plotted in Fig. 5. Obviously, the ntg'tttt band shifted to a higher wavenumber with decreasing temperature. Generally, under HP, molecular hardening was estimated using higher wavenumber shifts [25,36]. Therefore, the ntg'tttt conformer was extensively losing MF at LT. Meanwhile, there was no conformational change in the β–γ PT upon cooling at T_{C3} (= 183 K). Despite monoclinic–triclinic PT, the conformational changes were suppressed. In this study, we deduce that PT occurred only with molecular orientational and positional orders. Another possible reason is that the ntg'tttt hardening had a pinning effect to prevent conformational changes. In [C_8mim][PFBS], the nanoheterogeneous hardening and softening in a unit cell could be realized considering the temperature dependences of the Raman band shifting (Fig. 5). With the temperature decreasing to 100 K, both the crystal structures and molecular conformations were unchanged. Upon heating, an increase the all *trans* band was observed at 200 K ($> T_{C3}$), and a γ-β PT occurred reversely [33]. Similar to theβ-γ PT upon cooling, the conformers did not change at 200 K upon heating. Thus, a reversible β-γ PT could be explained by the molecular orientational and positional orders without conformational changes. Notably, the δ phase, which was not formed upon cooling, appeared with additional Bragg reflections at T_{C4} [33]. On the Raman spectra, there were trivial changes at 230 K ($> T_{C4}$). Thus, it is considered that the β-δ PT is derived only from molecular reorientations and position shifting. The heating-inherent δ phase caused

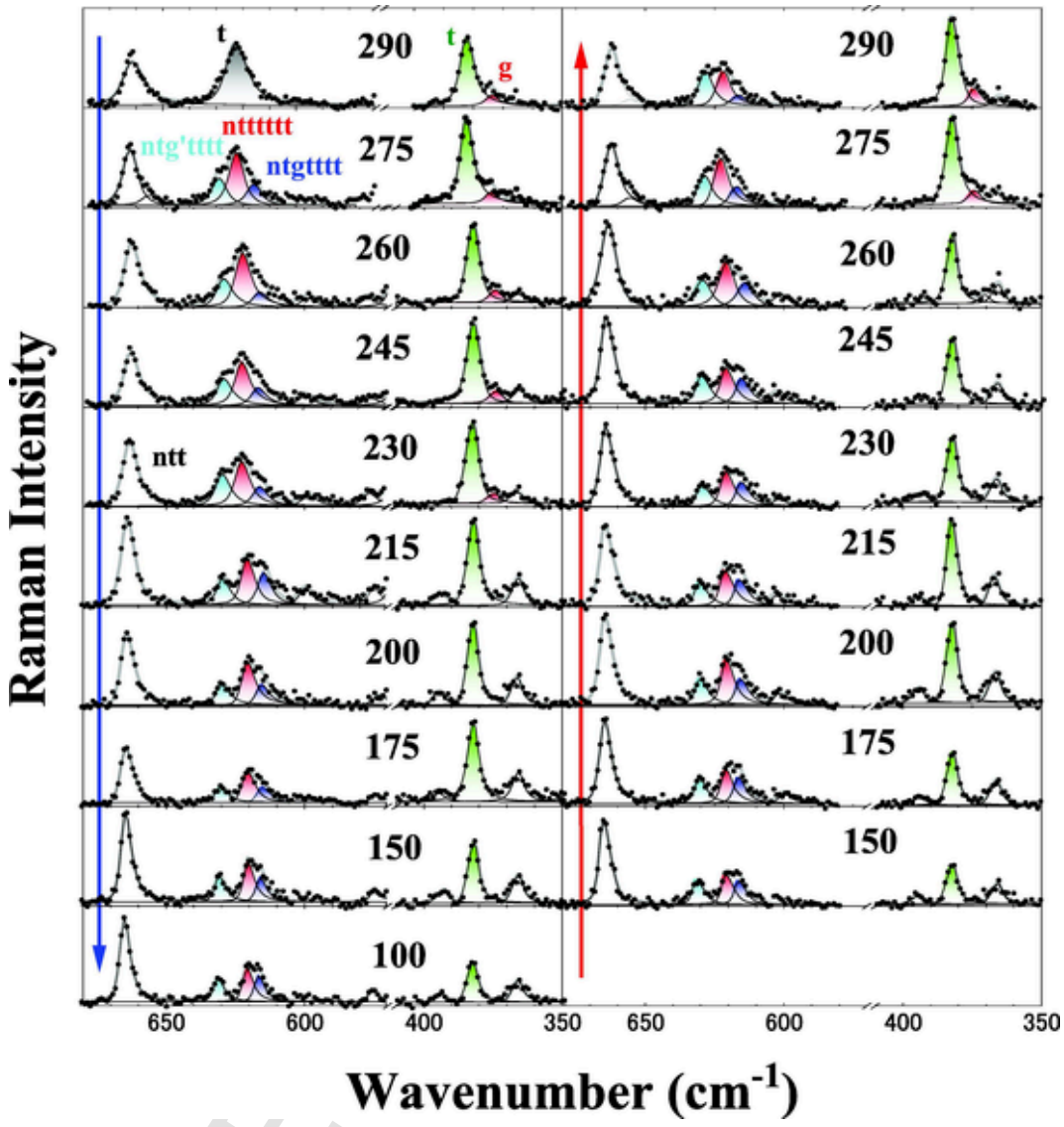

Fig. 4. Temperature dependences of Raman spectra of [C_8mim][PFBS] upon cooling and heating. Spectrum changes correspond to LT crystal polymorphs. The numbers in the figure indicate temperatures.

a δ-α PT at 290 K ($>T_{C2}$) accompanying the conformational changes (Fig. 4). At room temperature, the MF recovered and the *gauche* [PFBS]$^-$ band partially existed. We notice that *gauche* [PFBS]$^-$ is regarded as an indicator of the MF.

The LT phase behaviors of [$C_n$mim][PFBS] (n = 4, 6, and 8) are summarized in Table 1 and Fig. 5. The conformational traces in Fig. 6 are significant to interpret the conformation-driven LT crystal polymorphs. Not only in the solid state but also in the liquid state, we can extract the intrinsic properties of the cation conformers. In [C_4mim]$^+$, the *trans* and *gauche* liquid conformers contributed to the LT crystal polymorphs. An additional intermediate conformer of [C_6mim]$^+$ was first observed as the crossover behavior from the ionic to organic nature. However, only *trans* conformer was attributed to the LT crystal polymorphs. Meanwhile, only the *trans* conformer of [C_8mim]$^+$ was observable in the supercooled liquid state. Reflecting the long alkyl chain length, the conformational changes in [C_8mim]$^+$ were restricted at LT. In addition, the T_{NAT} values in Table 1 indicate the MF. In this study, based on XRD and DSC [33], we can clarify the phase varieties of [$C_n$mim][PFBS], which were driven by conformational polymorphs.

4. Conclusions

Cation and anion conformations of [$C_n$mim][PFBS] (n = 4, 6, and 8) were identified by RS, relating to LT crystal polymorphs. In the supercooled liquid state of [C_8mim][PFBS], both specific cation and anion conformers were observed. Complicated conformational variances with PTs appeared in [$C_n$mim][PFBS] upon both cooling and heating. The alkyl chain length effect for crystal polymorphs was clearly extracted: (i) conformational varieties of [C_4mim]$^+$ having a short alkyl chain correspond to MF, (ii) the *trans* dominant [C_8mim]$^+$ with a long alkyl chain length excluded *gauche*-like formations permitting partial hardening at LT, and (iii) [C_6mim]$^+$ possessing a crossover alkyl chain length indicated intermediate phase behaviors at LT. The complicated LT crystal polymorphs of [$C_n$mim][PFBS] originated from conformational polymorphs, MF, and molecular packing efficiency.

Uncited reference

[20].

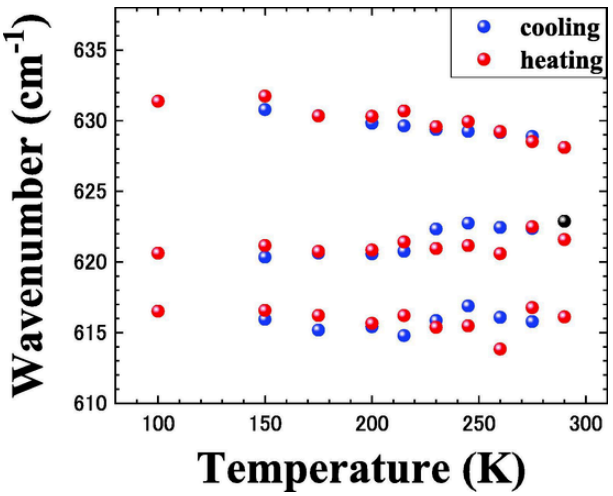

Fig. 5. Temperature dependence of wavenumber shifts of Raman bands. The nt-g'tttt Raman band shifted to a higher wavenumber with decreasing temperature.

Table 1
Conformational features of both cations and anion in the liquid and solid states. The non-all *trans* (NAT) bands exceeded the all *trans* bands at T_{NAT}.

	$[C_n mim]^+$				$[PFBS]^-$
		t	i	g	*I*(t): *I*(g)
Liquid (290 K)	$n = 4$	○	×	○	2: 1
	$n = 6$	○	○	○	2: 1
	$n = 8$	○	×	×	5: 1
		all *trans*	T_{NAT}		*gauche*
Solid (100 K)	$n = 4$	smallest	230 K		○
	$n = 6$	smallest	175 K		×
	$n = 8$	largest	–		×

CRediT authorship contribution statement

Hiroshi Abe : Conceptualization, Writing – original draft, Writing – review & editing. **Hiroaki Kishimura :** Data curation. **Mikio Uruichi :** Data curation.

Declaration of Competing Interest

The authors declare that they have no known competing financial interests or personal relationships that could have appeared to influence the work reported in this paper.

Data availability

Data will be made available on request.

Acknowledgments

We thank Dr. T. Takekiyo and Prof. Y. Yoshimura of the National Defense Academy for helpful discussion. We acknowledge Institute for Molecular Science, supported by the Nanotechnology Platform Program (JPMXP09S21MS1084) of the Ministry of Education, Culture, Sport, Science and Technology (MEXT), Japan.

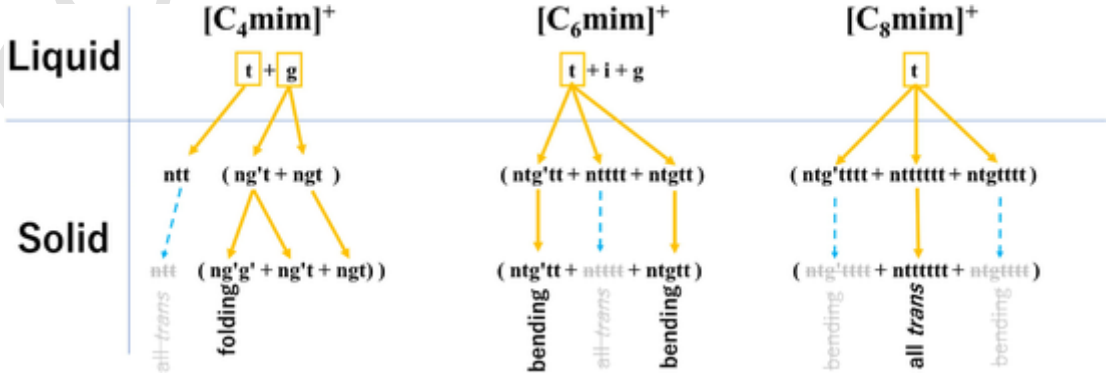

Fig. 6. Conformational traces from liquid to solid states upon cooling.

Appendix A. Supplementary data

Supplementary data to this article can be found online at https://doi.org/10.1016/j.saa.2022.121948.

References

[1] A. Nangia, Conformational Polymorphism in Organic Crystals, Acc. Chem. Res. 41 (5) (2008) 595–604.
[2] A.N. Sokolov, D.C. Swenson, L.R. MacGillivray, Conformational polymorphism in a heteromolecular single crystal leads to concerted movement akin to collective rack-and-pinion gears at the molecular level, Proc. Natl. Acad. Sci. 105 (6) (2008) 1794–1797.
[3] C. Greenwell, J.L. McKinley, P. Zhang, Q. Zeng, G. Sun, B. Li, S. Wen, G.J.O. Beran, Overcoming the difficulties of predicting conformational polymorph energetics in molecular crystals via correlated wavefunction methods, Chem. Sci. 11 (8) (2020) 2200–2214.
[4] A.J. Cruz-Cabeza, J. Bernstein, Conformational Polymorphism, Chem. Rev. 114 (4) (2014) 2170–2191.
[5] G.J.O. Beran, Modeling Polymorphic Molecular Crystals with Electronic Structure Theory, Chem. Rev. 116 (2016) 5567–5613.
[6] A.J. Cruz-Cabeza, N. Feeder, R.J. Davey, Open questions in organic crystal polymorphism, Commun. Chem. 3 (2020) 142–144.
[7] S.L. Price, From crystal structure prediction to polymorph prediction: interpreting the crystal energy landscape, Phys. Chem. Chem. Phys. 10 (2008) 1996–2009.
[8] S.Z. Ismail, C.L. Anderton, R.C.B. Copley, L.S. Price, S.L. Price, Evaluating a Crystal Energy Landscape in the Context of Industrial Polymorph Screening, Cryst. Growth Des. 13 (2013) 2396–2406.
[9] S.L. Price, Why don't we find more polymorphs? Acta Cryst. B 69 (4) (2013) 313–328.
[10] S.L. Price, D.E. Braun, S.M. Reutzel-Edens, Can computed crystal energy landscapes help understand pharmaceutical solids? Chem. Commun. 52 (2016) 7065–7077.
[11] S.L. Price, S.M. Reutzel-Edens, The potential of computed crystal energy landscapes to aid solid-form development, Drug Discovery Today 21 (2016) 912–923.
[12] P.G. Debenedetti, F.H. Stillinger, Supercooled liquids and the glass transition, Nature 410 (2001) 259–267.
[13] M.A. Neumann, J. van de Streek, F.P.A. Fabbiani, P. Hidber, O. Grassmann, Combined crystal structure prediction and high-pressure crystallization in rational pharmaceutical polymorph screening, Nature Commun. 6 (2015) 7793–7797.
[14] M. Vasileiadis, C.C. Pantelides, C.S. Adjiman, Prediction of the crystal structures of axitinib, a polymorphic pharmaceutical molecule, Chem. Eng. Sci. 121 (2015) 60–76.
[15] J. Hoja, H.-Y. Ko, M.A. Neumann, R. Car, R.A. DiStasio Jr., A. Tkatchenko, Reliable and practical computational description of molecular crystal polymorphs, Sci. Adv. 5 (2019) eaau3338–9.
[16] A.J. Cruz-Cabeza, E. Taylor, I.J. Sugden, D.H. Bowskill, S.E. Wright, H. Abdullahi, D. Tulegenov, G. Sadiq, R.J. Davey, Can solvated intermediates inform us about nucleation pathways? The case of β-pABA, CrystEngComm 22 (43) (2020) 7447–7459.
[17] S. Beil, M. Markiewicz, C.S. Pereira, P. Stepnowski, J. Thöming, S. Stolte, Toward the Proactive Design of Sustainable Chemicals: Ionic Liquids as a Prime Example, Chem. Rev. 121 (2021) 13132–13173.
[18] F. Philippi, T. Welton, Targeted modifications in ionic liquids – from understanding to design, Phys. Chem. Chem. Phys. 23 (12) (2021) 6993–7021.
[19] V.H. Paschoal, L.F.O. Faria, M.C.C. Ribeiro, Vibrational Spectroscopy of Ionic Liquids, Chem. Rev. 117 (10) (2017) 7053–7112.
[20] S. Dasari, B.S. Mallik, Conformational Free-Energy Landscapes of Alanine Dipeptide in Hydrated Ionic Liquids from Enhanced Sampling Methods, J. Phys. Chem. B 124 (2020) 6728–6737.
[21] F. Philippi, D. Pugh, D. Rauber, T. Welton, P.A. Hunt, Conformational design concepts for anions in ionic liquids, Chem. Sci. 11 (25) (2020) 6405–6422.
[22] S. Tsuzuki, A.A. Arai, K. Nishikawa, Conformational Analysis of 1-Butyl-3-methylimidazolium by CCSD(T) Level Ab Initio Calculations: Effects of Neighboring Anions, J. Phys. Chem. B 112 (26) (2008) 7739–7747.
[23] T. Endo, T. Higuchi, Y. Kimura, DFT Study on Conformation of 1-Alkyl-3-methylimidazolium with Ethyl, Propyl, Butyl, Pentyl, and Hexyl Group, Bull. Chem. Soc. Jpn. 93 (6) (2020) 720–729.
[24] S. Bilgili, F. Bardak, E. Kose, A. Atac, Investigation of the interionic interactions and spectroscopic features of 1-Octyl-3-methylimidazolium chloride, tetrafluoroborate, and hexafluorophosphate ionic liquids: An experimental survey and DFT modeling, J. Mol. Struct. 1261 (2022) 132912–213294.
[25] H. Abe, T. Takekiyo, N. Hatano, M. Shigemi, N. Hamaya, Y. Yoshimura, J. Phys. Chem. B 118 (2014) 1138–1145.
[26] H. Abe, T. Takekiyo, M. Aono, H. Kishimura, Y. Yoshimura, N. Hamaya, Polymorphs in room-temperature ionic liquids: Hierarchical structure, confined water and pressure-induced frustration, J. Mol. Liq. 210 (2015) 200–214.
[27] H. Abe, M. Aono, T. Takekiyo, Y. Yoshimura, A. Shimizu, Phase behavior of water-mediated protic ionic liquid: Ethylammonium nitrate, J. Mol. Liq. 241 (2017) 301–307.
[28] H. Abe, N. Hamaya, Y. Koyama, H. Kishimura, T. Takekiyo, Y. Yoshimura, D. Wakabayashi, N. Funamori, K. Matsuishi, Long Periodic Structure of a Room-Temperature Ionic Liquid by High-Pressure Small-Angle X-Ray Scattering and Wide-Angle X-Ray Scattering: 1-Decyl-3-Methylimidazolium Chloride, ChemPhysChem 19 (2018) 1441–1447.
[29] H. Abe, T. Takekiyo, Y. Yoshimura, A. Shimizu, S. Ozawa, Multiple crystal pathways and crystal polymorphs in protic ionic liquids, J. Mol. Liq. 269 (2018) 733–737.
[30] H. Abe, T. Takekiyo, Y. Yoshimura, N. Hamaya, S. Ozawa, Crystal Polymorphs and Multiple Crystallization Pathways of Highly Pressurized 1-Ethyl-3-Methylimidazolium Nitrate, Aust. J. Chem. 72 (2019) 87–92.
[31] H. Abe, H. Kishimura, T. Takekiyo, Y. Yoshimura, N. Hamaya, Non-equilibrium protic and aprotic ionic liquids: Measuring the distance from the equilibrium state, J. Mol. Liq. 283 (2019) 196–207.
[32] H. Abe, H. Kishimura, T. Takekiyo, T. Hanasaki, Y. Yoshimura, N. Hamaya, Low-temperature and high-pressure phase changes of room temperature ionic liquids, J. Mol. Liq. 300 (2020) 112340–112349.
[33] Y. Koyama, S. Shimono, H. Abe, K. Matsuishi, Crystal polymorphs in 1-alkyl-3-methylimidazolium perfluorobutanesulfonate ionic liquids, J. Mol. Liq. 317 (2020) 113908–1113907.
[34] H. Abe, Y. Koyama, H. Kishimura, K. Matsuishi, High-pressure crystal polymorph of the protic ionic liquid: Ethylammonium nitrate, J. Mol. Liq. 318 (2020) 113959–1113956.
[35] H. Abe, Phase variety in ionic liquids: Hydrogen bonding and molecular conformations, J. Mol. Liq. 332 (2021) 115189–1115127.
[36] Y. Koyama, S. Shimono, H. Kishimura, T. Takekiyo, Y. Yoshimura, H. Abe, K. Matsuishi, High-pressure crystal polymorphs in 1-butyl-3-methylimidazolium perfluorobutanesulfonate, J. Mol. Liq. 335 (2021) 116415–116417.
[37] H. Abe, Y. Koyama, S. Shimono, H. Kishimura, K. Matsuishi, High-pressure crystal polymorphs and multiple pathways in 1-hexyl-3-methylimidazolium perfluorobutanesulfonate ionic liquid, Chem. Phys. 557 (2022) 111479–1111477.
[38] K. Shimizu, A.A. Freitas, J.N. Canongia Lopes, Structural characterization of the $[C_nC1im][C_4F_9SO_3]$ ionic liquid series: Alkyl versus perfluoroalkyl side chains, J. Mol. Liq. 226 (2017) 28–34.
[39] S. Tsuzuki, T. Umecky, H. Matsumoto, W. Shinoda, M. Mikami, Interactions of Perfluoroalkyltrifluoroborate Anions with Li Ion and Imidazolium Cation: Effects of Perfluoroalkyl Chain on Motion of Ions in Ionic Liquids, J. Phys. Chem. B 114 (2010) 11390–11396.
[40] A.B. Pereiro, M.J. Pastoriza-Gallego, K. Shimizu, I.M. Marrucho, J.N. Canongia Lopes, M.M. Piñeiro, L.P.N. Rebelo, On the Formation of a Third, Nanostructured Domain in Ionic Liquids, J. Phys. Chem. B 117 (2013) 10826–10833.
[41] M.L. Ferreira, M.J. Pastoriza-Gallego, J.M.M. Araújo, J.N. Canongia Lopes, L.P.N. Rebelo, M.M. Piñeiro, K. Shimizu, A.B. Pereiro, Influence of Nanosegregation on the Phase Behavior of Fluorinated Ionic Liquids, J. Phys. Chem. C 121 (2017) 5415–5427.
[42] A.A. Granovsky, Firefly version 8, www.http://classic.chem.msu.su/gran/firefly/index.html.
[43] M.W. Schmidt, K.K. Baldridge, J.A. Boatz, S.T. Elbert, M.S. Gordon, J.H. Jensen, S. Koseki, N. Matsunaga, K.A. Nguyen, S. Su, T.L. Windus, M. Dupuis, J.A. Montgomery Jr, General atomic and molecular electronic structure system, J. Comput. Chem. 14 (1993) 1347–1363.
[44] S. Hayashi, R. Ozawa, H.-o. Hamaguchi, Raman Spectra, Crystal Polymorphism, and Structure of a Prototype Ionic-liquid [bmim]Cl, Chem. Lett. 32 (6) (2003) 498–499.
[45] T. Endo, T. Kato, K. Tozaki, K. Nishikawa, Phase Behaviors of Room Temperature Ionic Liquid Linked with Cation Conformational Changes: 1-Butyl-3-methylimidazolium Hexafluorophosphate, J. Phys. Chem. B 114 (2010) 407–411.
[46] S. Ozawa, H. Kishimura, S. Kitahira, K. Tamatani, K. Hirayama, H. Abe, Y. Yoshimura, Chem. Phys. Lett. 613 (2014) 122–126.
[47] H. Abe, R. Fukushima, M. Onji, K. Hirayama, H. Kishimura, Y. Yoshimura, S. Ozawa, J. Mol. Liq. 215 (2016) 417–422.